Chapter 3

Hydrogen Bond Synthons in the Interplay of Solubility and Membrane Permeability in Variable Stoichiometry Drug Cocrystals

3.1 Abstract

Four variable stoichiometry cocrystals of bronchodilator drug theophylline were synthesized with *o*-aminobenzoic acids along with 1:1 ratio cocrystal of *m*- & *p*-aminobenzoic acids. All materials were characterized by using different thermal, spectroscopic and X-ray diffraction techniques. Aqueous solubility and membrane permeability exhibited by these cocrystals were estimated. Structure-activity relationship is assessed to understand the interplay between various factors and the role of hydrogen bond synthon formation on the overall efficacy of the cocrystals. Hirshfeld surface analysis was further corroborated to examine drug−coformer and solute···solvent interactions in stoichiometry cocrystals that influences the resultant property.

3.2 Introduction

Design of cocrystal relies on hydrogen bond donor-acceptor ratios; however, the crystallization outcome may differ depending on the experimental conditions [1–5]. There are examples where stoichiometry of cocrystals varies irrespective of starting material ratio taken. Identifications of the factors and conditions such as solvent polarity, temperature, pressure which influences the formation of different stoichiometry cocrystal is imperative. Few research groups have attempted to understand the mechanism of different stoichiometry cocrystal [1–6]. Jones et al. studied 1:1 nicotinamide.suberic acid cocrystal formation as an intermediate while synthesizing 1:2 cocrystals. They emphasized the importance of mechanochemical grinding experiments to control cocrystal stoichiometry [1,2]. Jayasankar et al. studied solution mediated stoichiometry variation in cocrystals resulted from carbamazepine (CBZ) and *p*-aminobenzoic acid (*p*-ABA) 2:1 and 1:1 cocrystal [4]. They used reaction crystallization method (RCM) to synthesize the cocrystals by varying the concentration of the coformer in solution and demonstrated the dependence of cocrystal stability on coformer solution concentrations. Leyssens et al. recognized the solvent effects on the formation of urea:succinic acid (1:1 & 2:1) stoichiometry cocrystals [5]. The solid stoichiometric interconversion and

solvent-mediated conversion for pyrazinamide·*p*-nitrobenzoic acid with two stoichiometric cocrystals in a 1:1 and 2:1 ratio are also reported [7]. Recent work published from our group demonstrated the role of weak intermolecular interactions that direct the formation of different stoichiometry cocrystals [8]. Sarma et al. reported the role of π-stacking and hydrogen bond synthons in alteration of cocrystal stoichiometries [9]. The crystallization of phloroglucinol and phenazine yielded three different stoichiometry cocrystals viz. 1:1.5, 1:1.75, and 1:2 along with one 1:2:H_2O cocrystal solvate. It is one of the earlier examples of a cocrystal system with more than two stoichiometries. Formation of 1:1.75, and 1:2, 1:2:H_2O can be perceived on the insertion of extra phenazine molecule in crystal lattice directed by π-stacking. Friŝĉić et al. synthesized two 1:1 and 2:1 cocrystal of methyldiphenylphosphine oxide and 1,4-diiodotetrafluorobenzene which exhibit different supramolecular interactions [10]. The 1:1 cocrystal exhibit I···O halogen bonding along with and I···π interactions, whereas 2:1 cocrystal possess C–H···O hydrogen bonding. It is difficult to control the stoichiometry of a cocrystal system as the stoichiometry depends on the experimental conditions. There are limited literatures which emphasis on cocrystal stoichiometry control techniques. Trask et al. reported that it was possible to obtain 1:2 caffeine acetic acid cocrystals by applying both solution crystallization and solid state neat grinding method, however, the 1:1 cocrystal resulted only from solid state neat grinding [1]. Solvent-free continuous cocrystallization (SFCC) demonstrated as one of the successful techniques in controlling the stoichiometry of caffeine and maleic acid cocrystal [11]. Recently, gel crystallization strategy was reported by Mei et al. to control the stoichiometry of vitamin C (VC) cocrystal [12].

Study on the physiochemical property such as stability, solubility, dissolution is equally imperative in drug cocrystal formulation perspective [13–17]. Cocrystals of caffeine and acetic acid in different stoichiometry (1:1 and 1:2) possess different physical stability that has been described based on crystal packing differences [1]. For multiple stoichiometry cocrystal systems as the ratio of more soluble coformer increases, it is expected to favour dissolution [4]. However, cocrystal with highest soluble coformer does not necessarily display higher dissolution. Recently, Matzger *et al.* accessed the dissolution and solubility behavior with respect to coformer concentration considering carbamazepine (CBZ)/ *p*-aminobenzoic acid (PABA) 1:1 and 2:1 and 4:1 cocrystal and

compared with different weak intermolecular interactions in its crystal lattice [6]. Corner *et al.* reported a case study of property prediction and pharmacokinetic evaluation of mixed stoichiometry cocrystals of asthma drug Zafirlukast with piperazine [18].

Despite being the availability of few reports on different stoichiometry cocrystal that showing different properties, a study on the structure-property relationship of various stoichiometry cocrystals of a drug with the same coformer based on hydrogen bond interaction pattern is important and thereby the scope of the present chapter. This chapter is focused on the synthesis of different stoichiometry cocrystals of theophylline (THP) using crystal engineering approach [19]. Three commonly used and readily available coformers, i.e. isomeric aminobenzoic acids [*o*-Aminobenzoic acid (*o*-ABA), *m*-Aminobenzoic acid (*m*-ABA); *p*-Aminobenzoic acid (*p*-ABA)] are considered to prepare the cocrystal materials with THP.

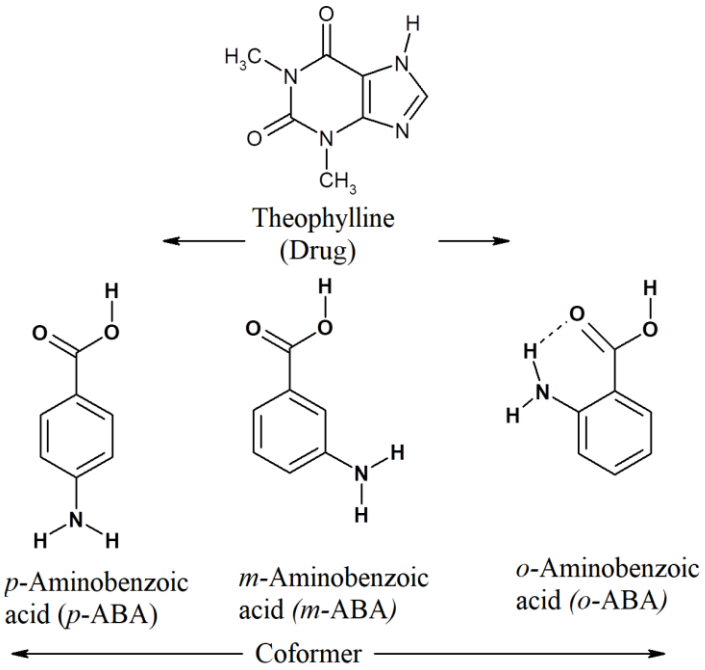

Scheme 3.1 Chemical structures of drug theophylline and the isomeric aminobenzoic acid coformers.

Isomeric aminobenzoic acids are also known to possess biological activities; primarily in metabolic processes and phytotoxicity. Spectroscopy, thermal analysis, powder X-ray diffraction, and single crystal X-ray structure determination are employed to characterize all cocrystals materials. The synthesized cocrystals materials are further subjected to aqueous solubility and diffusion/membrane permeability analysis. The role of solubility

and permeation product behaviour of the drug, i.e. the effective drug bioavailability is emphasized on the basis of different energy supramolecular synthon formation and solute···solvent interactions exhibited by the stoichiometry cocrystals.

3.3 Results and Discussion

3.3.1 Synthesis of Cocrystals

Based on crystal engineering principles four different stoichiometry cocrystals of the THP·*o*-ABA system were synthesized including hydrates and *iso*-BuOH solvate. Detail synthetic procedures are available in the experimental section 3.5.2. The THP imidazole NH group acts as a hydrogen-bond donor and imidazole N with two C=O groups can act as hydrogen-bond acceptors, and thereby making THP a 1 donor 3 acceptors molecule [=CH weak donor]. The –COOH and $–NH_2$ groups in the coformer offer the formation of O–H···O, N–H···O, N–H···N and O–H···N hydrogen bonds [20–24]. Possible supramolecular synthon formation between them is discussed in Chapter 2 and analysed by CCDC. The coformer *m*-ABA and *p*-ABA show availability of 1 acceptor and 3 donors. Thus, it is easily predictable of 1:1 cocrystal formation. But *o*-ABA has one O–H and N–H donor and one C=O acceptor that decides the variable number of symmetry independent entities of drug and coformer in the asymmetric unit. The inclusion of polar solvents and/or water in the lattice of THP·*o*-ABA cocrystals is possible to adjust hydrogen bond donor-acceptor ratios (Table 3.1).

Table 3.1 Isomeric aminobenzoic acids (ABA) cocrystallized with drug theophylline (THP) resulted in different stoichiometry cocrystals with *o*-Aminobenzoic acid. Water and/or solvent inclusion is observed as a compensator for donor-acceptor ratios. The *m*- and *p*- Aminobenzoic acid produce only 1:1 cocrystal.

Drug	Coformer	Cocrystal	Stoichiometry THP:ABA	Solvent inclusion
Theophylline (THP)	*o*-Aminobenzoic acid	CC-I	2:3	-
		CC-II	2:2	2 *iso*-BuOH
		CC-III	3:2	4 H_2O
		CC-IV	2:1	4 H_2O
	m-Aminobenzoic acid	CC-V	1:1	
	p-Aminobenzoic acid	CC-VI	1:1	–

3.3.2 Characterization

FT-IR spectra were recorded for solid samples of the cocrystal materials to understand the formation of intermolecular hydrogen bonding between different functional groups (details are in experimental section 3.5.3. From the FT-IR spectra, significant peak shifting is observed for all the cocrystal materials, which further indicates the formations of intermolecular hydrogen bonding (Figure 3.1). The band at ~1700 cm^{-1} represented the carbonyl C=O stretching i.e., C=O in cocrystals. Prominent characteristic peaks between 3600 and 3440 cm^{-1}, is assigned to stretching vibration of the O−H group. The broad band at 3500–3350 cm^{-1} is assigned for the N−H stretching vibration. The band at 2500 cm^{-1} is due to the O−H group of the carboxylic acid. The 1650–1600 cm^{-1} band is assigned to N–H bending vibration of coformers. The peaks at 1300–1250 cm^{-1} suggested bending vibration of the O–H group, which indicates the presence of carboxylic acid. The peak in the region 950–900 cm^{-1} suggested the N−H bending vibration of the amine group.

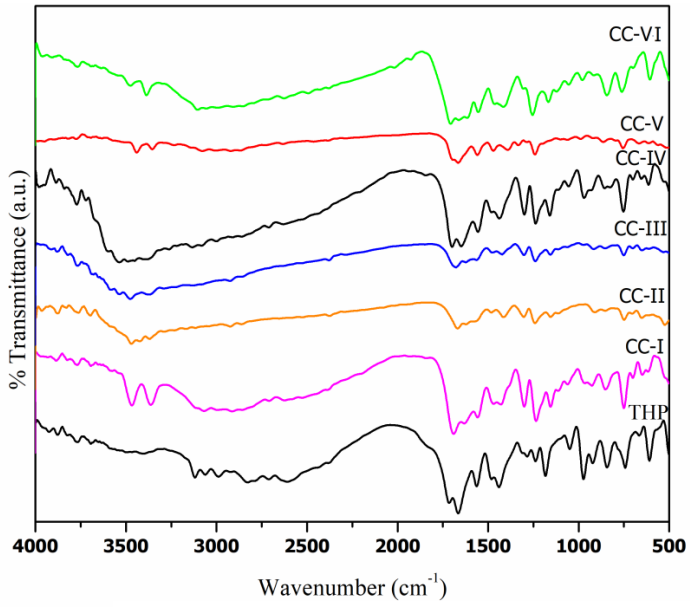

Figure 3.1 FT-IR comparison of cocrystals of THP-ABA (CC-I to CC-VI).

PXRD has been recorded for all the cocrystal materials. The experimental PXRD patterns of CC-I to CC-VI cocrystal materials are compared with those simulated from the single-crystal structures data, which are discussed in the subsequent section (Figure 3.2). The overlaid patterns generated from single crystal structure and experimental PXRD patterns showed the same peak position and intensity profile. A good agreement

with the simulated pattern indicated the purity of the phase. Overlay patterns are presented in the Appendix Figure A.4.

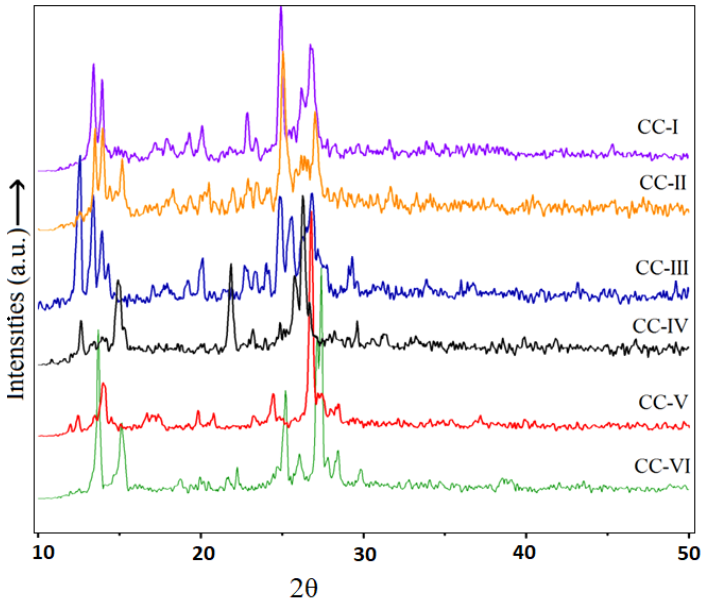

Figure 3.2 Powder X-ray diffraction patterns of cocrystals CC-I to CC-VI.

TGA & DSC analysis was performed to study the thermal behaviour of the cocrystals. The endotherms of the cocrystals are presented in Figure 3.3 and onset melting points are tabulated in Table 3.2. The DSC thermogram of CC-I showed a single endothermic transition, which can be attributed to the melting transition (132.1 °C) of pure cocrystal material different from that of starting components. Similarly, single endothermic transition for the cocrystals CC-V and CC-VI respectively at 176.6 °C and 164 °C demonstrated new cocrystal phases and also indicated as pure non-solvated forms. The endothermic transitions between 60 °C and 120 °C for CC-II, CC-III and CC-IV indicated the loss of water or solvent molecules (*iso*-BuOH for CC-II) from the cocrystals. The peak appeared at 144-146 °C after the melting of CC–IV could be due to the presence of coformer *o*-ABA as an impurity. The melting points of the cocrystals somewhere in between melting point of the starting components, follow the common trend of 51% probability of getting the melting behaviour of cocrystal reported elsewhere [25]. Only CC-V is an exception with a similar melting point with the coformer (only 4% probability).

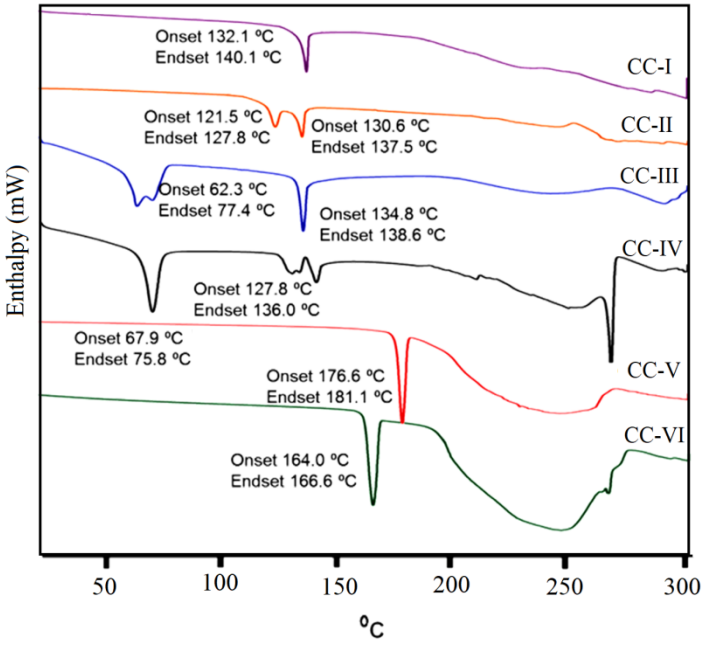

Figure 3.3 The DSC endotherms represent melting onset of the cocrystals CC-I to CC-VI. Onset temperatures within 120 °C are for solvate/hydrate release from cocrystal CC-II, CC-III and CC-IV.

Table 3.2 The endotherms representing the melting onset of the cocrystals and 60-125 °C for solvate/hydrate cocrystals (i.e. CC-II, CC-III and CC-IV) correspond to solvate/water release.

Drug	Coformer	Coformer melting temperature (°C)	Cocrystals	Water/solvent loss temperature (°C)		Cocrystal melting point (°C)	
				Onset	Peak	Onset	Peak
			CC-I	–	–	132.1	140.1
	o-ABA	144–146	CC-II	121.5	127.8	130.6	137.5
THP			CC-III	62.3	77.4	134.8	138.6
[M.P.			CC-IV	67.9	75.8	127.8	136.1
~271°C]	*m*-ABA	178–180	CC-V	–	–	176.6	181.1
	p-ABA	187-189	CC-VI	–	–	164.0	166.6

TGA endotherms of CC-III and CC-IV showed weight loss of 12.3% (calculated12.6%)and 8.3% (calculated 8.2%) that agreed well with predicted values due to evaporation of water molecules in the temperature range 60-100 °C respectively. Weight loss of 18.7% (calculated18.9%) for CC-II at temperature range 110-125 °C

confirmed the release of higher boiling solvents i.e. two molecules of *iso*-BuOH from the crystal lattice (Figure 3.4).

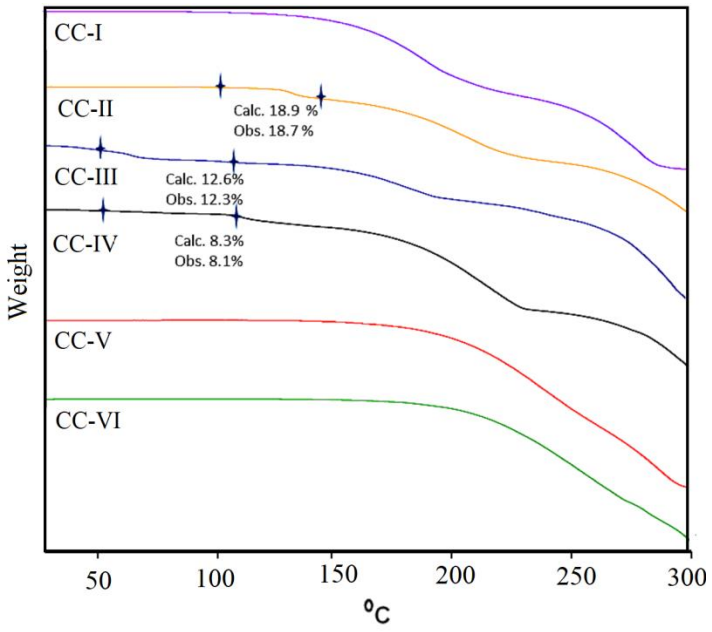

Figure 3.4 Weight loss measured by TGA found in good agreement with the theoretical values due to the evaporation of two *iso*-BuOH molecule for CC-II and four water molecules from CC-III and CC-IV cocrystals.

Single crystal X-ray structures for all cocrystals were determined and analysed the supramolecular synthon formed between THP and coformers (Details are in experimental section 3.5.6). Crystal data parameters for CC-I to CC-VI are summarized in Appendix Table A.4. The guest-free crystalline modification with pink block crystals of CC-I was isolated from ethanol (Table 3.5). It crystallized in triclinic space group $P\bar{1}$ with 2 THP and 3 *o*-ABA symmetry independent molecules in the crystal lattice. Two symmetry independent THP are hydrogen bonded by N−H···O homodimers (Figure 3.5). Two such dimers are connected by two symmetry independent *o*-ABA molecules via N−H···O, O−H···N and C−H···O interactions forming a channel along crystallographic [100] axis [calcd. void size 6.5 Å×4.4 Å]. The third crystallographic *o*-ABA molecule nicely fits in the channel. They are arranged in a 1D tape via N−H···O hydrogen bonds. These 1D tapes run roughly perpendicular to the 2D sheet [parallel to the (100) plane, blue circle] formed by THP dimers and *o*-ABA molecules. Hydrogen bond parameters are tabulated in Table 3.3.

In CC-II, the THP, N−H···O dimers are connected by *o*-ABA molecules leading to a helical 1D chain. Two such helices coiled each other and run in parallel along [010] axis leading to the formation of a channel [calculated. void size of 6.5 Å×4.4 Å] for solvent inclusion. The similarity between CC-I and CC-II is that [shown in blue circle for CC-I in Figure 3.5], 2 molecules of disordered *iso*-BuOH molecules are sitting in the void replacing the third *o*-ABA in CC-I (Figure 3.6). Disordered *iso*-BuOH molecules are removed from the crystal structure using PLATON SQUEEZE program for CIF clearance. The channel formation in CC-I and CC-II expresses similar structural trend that promotes inclusion of solvent/coformer molecules having similar size and identical hydrogen bond behaviour.

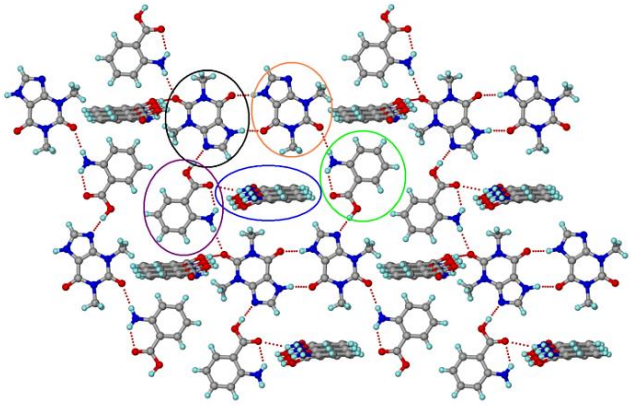

Figure 3.5 THP N−H···O dimer connected by *o*-ABA molecule leading to a 1D tape and then construct 2D sheet parallel to (100) plane in CC-I. Symmetry-independent molecules are spotted inside colour circles. The third crystallographic *o*-ABA molecule (blue circle) sits in the cavity formed by 2D sheets via N−H···O hydrogen bonds and runs almost perpendicular to the layer.

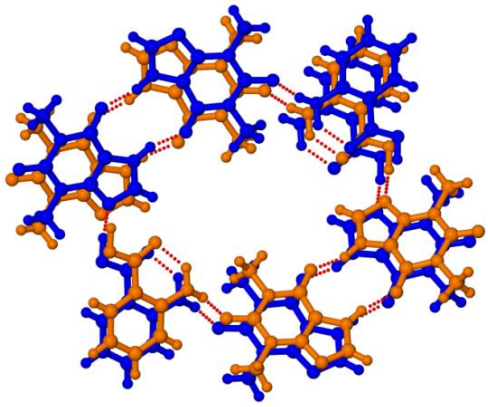

Figure 3.6 THP N−H···O homodimers are connected by *o*-ABA molecules through N−H···O and O−H···O interactions leading to a 1D helix in CC-II. Two such helices coiled and run along [010] axis leading to channels for solvent inclusion.

When, 2:1 ratio starting materials cocrystallized from pure water afforded CC-III, i.e. 3:2 cocrystals of THP and *o*-ABA with 4 molecules of water incorporation in the asymmetric unit. The crystal structure of CC-III is solved and refined in triclinic $P\bar{1}$ space group. The symmetry independent THP molecule forms N−H···O dimer to its inversely related molecule construct an identical 1D tape observed in CC-I (Figure 3.7a, ribbon 2, voids for solvent inclusion in blue colour). Two tetrameric units of THP molecules are connected by *o*-ABA molecules via carboxylic O−H···N and amine N−H···O afforded a

second type 1D molecular tape (ribbon 1, Figure 3.7a). Ribbon 1 also forms channels along [001] crystallographic axis for water inclusion (red circle in Figure 3.7a). Both ribbons are organized in ABAB… fashion and construct a molecular 2D sheet that further completes 3D packing by stacking (Figure 3.7a).

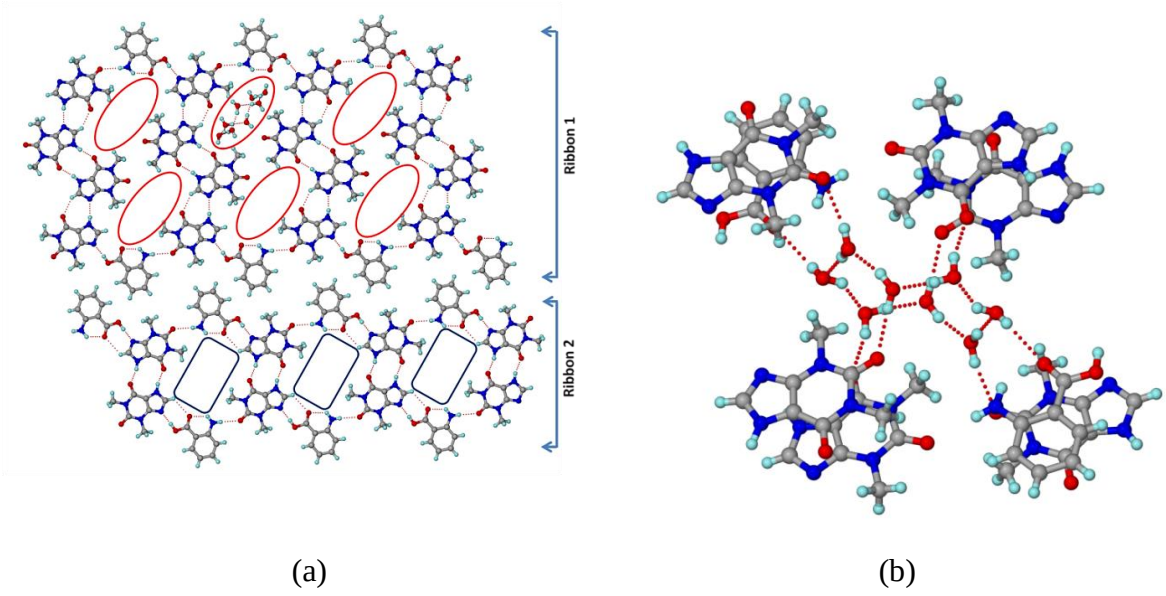

(a) (b)

Figure 3.7 (a) In CC-III, THP N−H···O dimers connected by *o*-ABA form similar 1D tape shown in structure CC-I. This ribbon 2 forms channel (blue rectangle) allows water inclusion. Other symmetry-independent THP molecule form tetrameric chain that further joined by *o*-ABA constructing another 1D molecular tape (ribbon 1). Red circles indicate the inclusion of water molecules. (b) Waters in void form octamer held by O−H···O interactions with THP and *o*-ABA.

Cocrystal CC-IV is isolated when THP mixed with *o*-ABA in 2:1 ratio and acetonitrile solvent drop grinding followed by methanol solution crystallization. This crystal structure is found to be solvated and refined in triclinic $P\bar{1}$ space group with 2 molecules of THP, one *o*-ABA and 4 molecules of water in the asymmetric unit. Molecular arrangement in the lattice shows a similar structure of ribbon 1 shown for structure CC-III with two different type void spaces filled by water molecules (Figure 3.8a). Water molecules are arranged in octamer for both CC-III and CC-IV structures (Figure 3.7b and 3.8b).

A layered structure without a cavity/channel for solvent inclusion is observed for CC-V and CC-VI [26]. The coformer m-ABA and p-ABA result 1:1 cocrystal with THP irrespective of starting ratios of drug-coformer and solvent of crystallization. The 1:1

cocrystal of THP·m-ABA, [i.e. CC-V] crystallized in monoclinic P21/c space group. The COOH of *m*-ABA is hydrogen bonded via O−H···O to pyrimidine carbonyl supported by strong auxiliary N−H···O interaction that forms hetero acid-amide like dimers (Figure 3.9a).

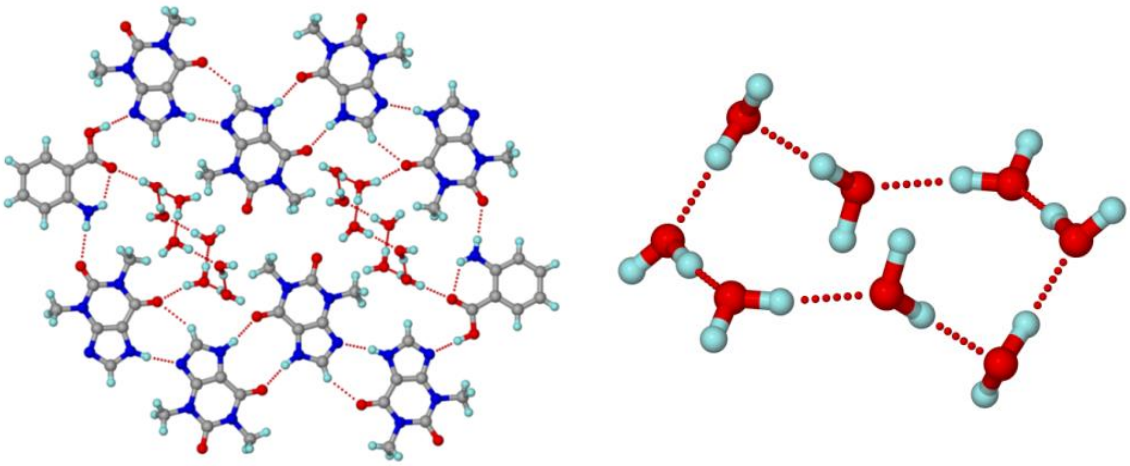

(a) (b)

Figure 3. 8 (a) The crystal structure of CC-IV shows exactly similar structure pattern as ribbon 2 for CC-III have shown in Figure 5a. (b) Water octamer held by O−H···O interactions fills the cavity.

The heterodimers are further connected by N−H···O interaction leading to a 1D chain. The COOH interaction to $N_{pyrimidine}$ is generally observed, however, the N−H···N interaction from NH_2 to the basic N of THP favours in this structure. Perhaps this N−H···N and C−H···O connect 1D tapes into a 2D sheet (Figure 3.9b). The C−H···π and π···π interactions play an important role in stacking the layers into a 3D molecular arrangement.

As anticipated, THP results in 1:1 neutral cocrystal with *p*-ABA without the inclusion of lattice solvent. The *p*-ABA carboxyl group forms heterodimer with THP pyrimidine NH and adjacent carbonyl moiety (Figure 3.10a). The NH_2 group is hydrogen bonded via N−H···O interaction to the second carbonyl group and forms a 1D tape. The C−H···O interaction holds the tapes to form a 2D sheet-like structure along *bc* plane (Figure 3.10b). They further stacked via weak C−H···O and π···π interactions along [100] axis to complete 3D arrangement of the molecules in the lattice.

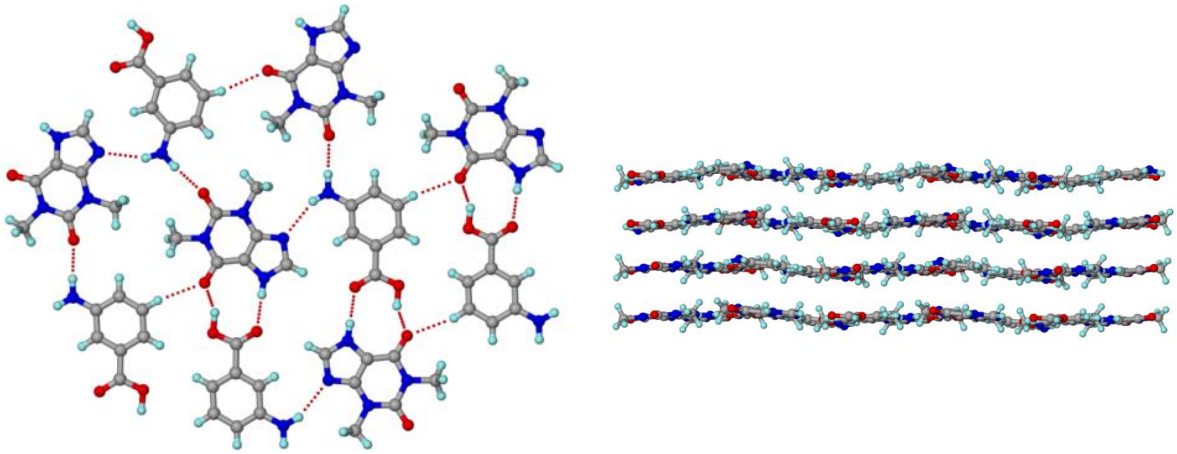

(a) (b)

Figure 3.9 (a) The acid-amide like heterodimers between THP and *m*-ABA are formed via O−H···O and N−H···O interactions. The NH_2 group connects the dimeric units via N−H···O and N−H···N interactions supported by C−H···O interaction construct 2D molecular layers. (b) Layers are further stacked via C−H···π and π···π into 3D packing.

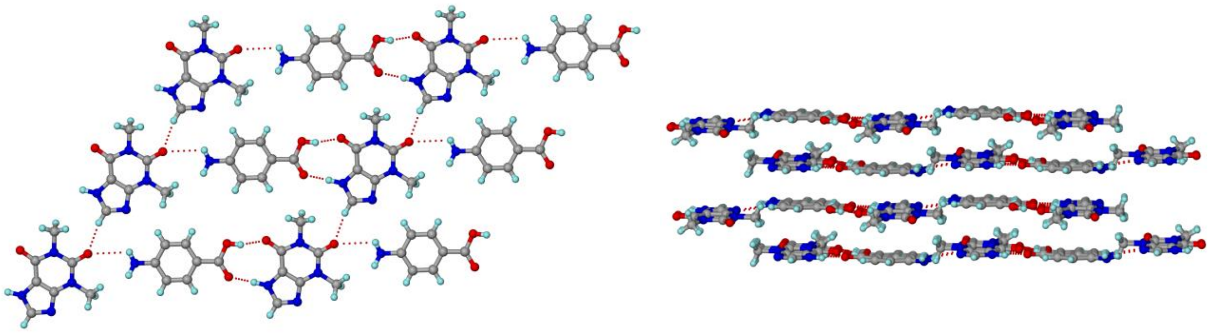

(a) (b)

Figure 3.10 (a) Pyrimidine NH of THP and adjacent C=O group form strong hydrogen bonds through O−H···O and N−H···O with COOH of *p*-ABA that further connects another heterodimer via NH_2, N−H···O form 1D molecular tape. Molecular tapes are connected by C−H···O, C−H···N and weak N−H···O hydrogen bonds resulted 2D sheets which piled up (b) to complete 3D molecular arrangements along crystallographic [100]-axis.

Table 3.3 Hydrogen bond parameter of **CC-I** to **CC-VI**

Cocrystal	Interaction	H···A/Å	D···A/Å	∠D–H···A/°	Symmetry code
CC-I	N_1–H_{1A}···O_4	1.82	2.741(2)	170	1-x,1-y,1-z
	O_5–H_{5A}···N_2	1.72	2.695(2)	174	1-x,2-y,-z
	N_6–H_6···O_2	1.75	2.705(2)	169	1-x,1-y,1-z
	O_8–H_{8A}···N_5	1.74	2.712(2)	177	1-x,1-y,1-z
	N_9–H_{9B}···O_3	2.45	3.306(3)	161	1-x,-y,1-z
	O_9–H_{9C}···O_3	1.67	2.661(2)	176	1+x,y,z
	N_{10}–H_{10A}···O_7	2.47	3.285(3)	153	—
	N_{10}–H_{10B}···O_{10}	2.19	3.002(3)	160	-1+x,y,z

	N_{11}–H_{11B}···O_1	2.16	3.046(3)	176	1-x,1-y,-z
	C_{13}–H_{13C}···O_{10}	2.58	3.509(3)	163	-1+x,y,z
	C_{19}–H_{19}···O_{10}	2.47	3.277(3)	145	-1+x,y,z
	C_{32}–H_{32}···O_{10}	2.46	3.243(3)	142	-1+x,y,z
	O_2–H_{2C}···N_8	1.76	2.726(4)	174	1-x,1-y,1-z
	N_3–H_{3A}···O_1	2.50	3.260(5)	151	—
	N_3–H_{3B}···O_6	2.24	3.069(5)	165	-1+x,y,z
	N_4–H_{4B}···O_8	1.90	2.740(5)	164	1-x,1-y,1-z
	O_5–H_{5A}···O_7	1.65	2.670(4)	169	—
	O_4–H_{5B}···N_5	1.76	2.700(4)	177	1-x,2-y,-z
	N_9–H_{9A}···O_9	1.73	2.714(5)	169	1-x,1-y,1-z
	C_{12}–H_{12}···O_6	2.51	3.313(5)	144	—
	C_{18}–H_{18}···O_6	2.59	3.376(4)	142	-1+x,y,z
CC-II	N_2–H_{2A}···O_3	1.79	2.728(3)	164	-1/2+x,1-y,-1/2+z
	N_6–H_{6D}···O_1	1.84	2.749(3)	155	1/2+x,1-y,1/2+z
	O_6–H_{6E}···N_5	1.66	2.715(3)	168	1-x,-y,1-z
	O_8–H_{8A}···N_1	1.60	2.668(3)	175	1-x,1-y,-z
	N_9–H_{9A}···O_2	2.02	3.019(3)	168	—
	N_{10}–H_{10A}···N_9	2.48	3.251(4)	155	x,1+y,z
CC-III	N_2 –H_{2A}···O_1	1.82	2.728(2)	165	1-x,1-y,-z
	N_6 –H_{6D}···N_9	2.07	2.873(3)	171	-x,1-y,1-z
	O_7 –H_{7D}···N_1	1.76	2.708(3)	178	-1+x,y,z
	O_{10} –H_{10A}···N_5	1.78	2.688(3)	173	1-x,1-y,1-z
	N_{10} –H_{10C}···O_5	1.83	2.789(2)	171	1-x,1-y,1-z
	O_{11} –H_{11A}···O_2	2.21	3.011(3)	166	—
	O_{11}–H_{11B}···O_{14}	1.90	2.736(3)	173	—
	O_{12}–H_{12A}···O_3	2.02	2.813(3)	158	-x,1-y,1-z
	O_{12}–H_{12B}···O_{13}	1.90	2.726(3)	169	x,1+y,z
	O_{13}–H_{13D}···O_6	2.06	2.857(3)	177	—
	O_{13}–H_{13E}···O_{11}	2.03	2.777(4)	153	-1+x,y,z
	N_{13}–H_{13F}···O_2	2.23	3.108(3)	176	-1+x,1+y,z
	N_{14}–H_{14E}···O_4	2.25	3.111(3)	174	1-x,-y,1-z
	O_{14}–H_{14F}···O_5	2.52	3.222(3)	142	—
	O_{14}–H_{14G}···O_{12}	2.02	2.718(3)	141	1-x,1-y,1-z
	C_{15}–H_{15}···O_3	2.38	3.178(3)	143	-x,1-y,1-z
CC-IV	O_1–H_{1A}···N_6	1.73	2.696(8)	176	1-x,-y,-z
	N_2–H_{2A}···O_6	1.85	2.772(9)	170	2-x,-y,-z
	N_5–H_{5A}···N_1	1.94	2.873(9)	171	1-x,1-y,-z

	$O_7–H_{7A}\cdots O_3$	1.86	2.789(8)	162	—
	$O_7–H_{7B}\cdots O_8$	1.81	2.738(11)	164	—
	$O_8–H_{8A}\cdots O_{10}$	1.91	2.811(11)	177	—
	$O_8–H_{8B}\cdots O_5$	1.97	2.892(10)	170	1-x,1-y,1-z
	$O_9–H_{9A}\cdots O_7$	1.86	2.718(12)	171	-x,1-y,1-z
	$O_9–H_{9B}\cdots O_2$	2.07	2.791(9)	143	1-x,-y,1-z
	$N_9–H_{9C}\cdots O_4$	2.13	3.006(10)	177	1-x,-y,1-z
	$O_{10}–H_{10A}\cdots O_9$	1.82	2.762(13)	171	1-x,-y,1-z
	$O_{10}–H_{10B}\cdots O_4$	2.20	3.043(10)	173	1-x,-y,1-z
	$C_8–H_8\cdots O_9$	2.59	3.479(12)	161	x,y,-1+z
	$C_{15}–H_{15}\cdots O_3$	2.38	3.181(10)	144	1-x,1-y,-z
CC-V	$N_4–H_{4A}\cdots O_6$	1.78	2.785(4)	177	1+x,1/2-y,1/2+z
	$O_5–H_{5A}\cdots O_1$	1.70	2.634(4)	157	-1+x,1/2-y,-1/2+z
	$N_9–H_{9A}\cdots O_2$	2.00	3.006(5)	174	1+x,y,z
	$N_9–H_{9B}\cdots N_1$	2.36	3.299(5)	154	2-x,1/2+y,1/2-z
CC-VI	$N2–H_{3A}\cdots O_1$	1.74	2.712(14)	179	1-x,1-y,1-z
	$O2–H_{5A}\cdots O_4$	1.78	2.683(12)	166	1-x,1-y,1-z
	$C12–H_{4A}\cdots O_3$	2.34	3.200(16)	147	x,1+y,z
	$C13–H_{13A}\cdots O_1$	2.59	3.238(17)	125	1-x,-y,1-z
	$C14–H_{14C}\cdots O_3$	2.52	3.332(15)	142	1-x,-y,-z

3.3.3 Phase Stability

The hydrate formation of a drug seems to occur oftentimes because of the awkward shape and availability of various polar functional groups. In spite of that, it is also observed that cocrystal technology can avoid water inclusion and phase transformation. For example, cocrystals of oxalic acid with API caffeine and theophylline are identified as kinetically stable even at 98% RH [27]. Cocrystals of flufenamic acid with THP, sorbic acid, etc. are few representative cocrystal systems demonstrated as stable upon slurring for several days [28,29]. To understand the possibility of phase transformation of pure cocrystals into either THP hydrate or other forms during solubility and membrane permeation study, we opted to perform a series of slurry experiments in water (details in experimental section). A definite amount of cocrystal slurry was taken out and air-dried for PXRD analysis at time intervals 1, 24, 48, and 72 h. The stacked plot of PXRD patterns (Figure 3.11 a, b) reveals that none of the examined cocrystals showed phase transformation. Experimental PXRD patterns exactly resembled the simulated

patterns generated from the crystal structure. Additionally, the absence of the intense peaks at 2θ, 11.66 and 27.60, responsible for THP hydrate, confirm that the cocrystals are quite stable and do not show THP hydrate formation up to 3 days.

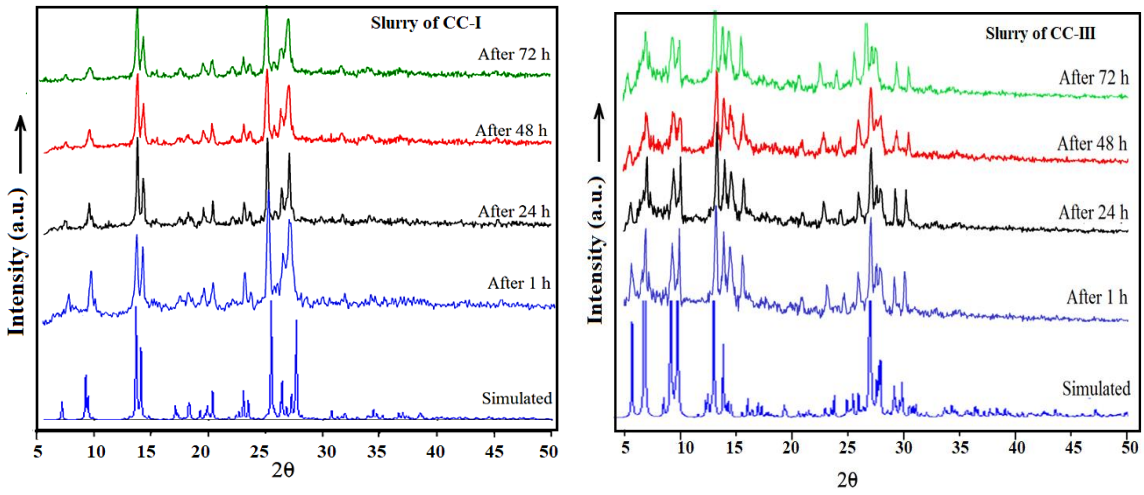

(a) (b)

Figure 3.11 Stacked plots of PXRD patterns recorded for the slurry of CC-I (a) and CC-III (b) prepared in water show no phase transformation even after 3 days.

3.3.4 Aqueous Solubility

Cocrystal solubility generally depends on complexation of components. Component concentrations and type of coformers used to play an important role in cocrystal solubility modulation. Generally, higher soluble coformers result in cocrystals with higher solubility. Solubility analysed for a series of cocrystals of carbamazepine, theophylline, caffeine etc. showed that the coformers should have multi-fold higher solubility than API to achieve higher soluble cocrystals [25-27]. Here, we introduced coformers with comparable to lesser aqueous solubility than the API (Table 3.4). All cocrystal materials showed higher solubility than that of both API as well as their respective coformers. The solubility data are consistent with the interpretation that enhanced solute⋯solvent interactions, responsible for higher aqueous solubility of the cocrystals (Figure 3.12). Needless to mention that, water incorporation decreases the solubility and in accordance with our results obtained for CC-III & CC-IV. Analysing crystal structures, we found that the water octamer clusters for both structures are embedded inside the API·*o*-ABA hydrogen bonded 2D molecular layers. The hydrophobic π-clouds of 2D molecular layers are exposed to the crystallizing media for

interactions. Moreover, the water clumps are strongly hydrogen bonded via O–H···O interaction while comparing weaker N–H···O in CC-I. Thereby remains a lesser possibility for solute···solvent interaction to show higher solubility in CC-III and CC-IV. Two OH groups of H_2O molecule in the octamer of CC-IV are in short contact with the API and *o*-ABA which explains in minor deviation in their solubility values. Lower aqueous solubility by CC-II is expected after analysing hydrophobic interactions by isobutyl groups with the solvent. The O–H···O single hydrogen bonding between guest and host in the structure compensated the hydrophobic nature and contributed towards a higher solubility than the hydrated structures.

Table 3.4 Aqueous solubility comparison of THP, coformers and cocrystals

Drug	Solubility (mg/mL)	Coformer	Solubility (mg/mL)	Cocrystal	Solubility (mg/mL)
THP	8.3	*o*-ABA	5.7	CC-I	98.90
				CC-II	45.73
				CC-III	26.09
				CC-IV	27.75
		m-ABA	5.9	CC-V	25.38
		p-ABA	4.7	CC-VI	23.68

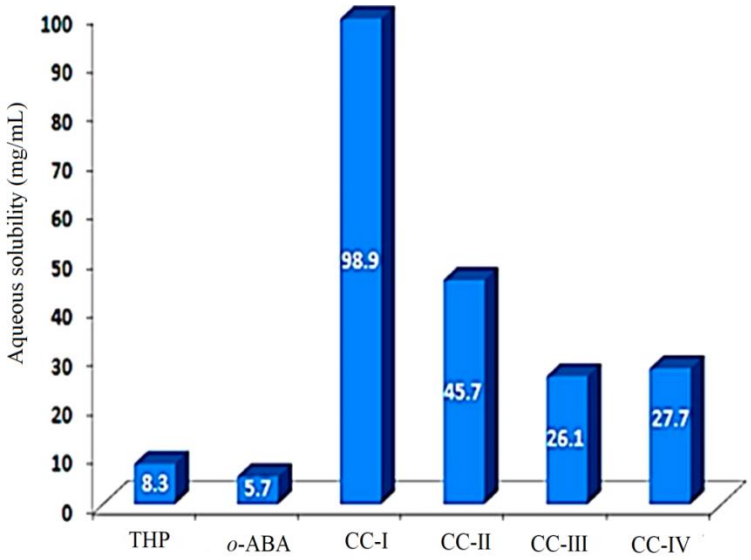

Figure 3.12 Graphical representation of aqueous solubility of the drug THP, coformer *o*-ABA and their variable stoichiometry cocrystals (CC-I, CC-II, CC-III and CC-IV).

3.3.5 Membrane Permeability

The trade-off between the apparent solubility increase and permeability decrease that can lead to paradoxical effects on the overall fraction of drug absorbed has been reported using solubility-modifying formulations as pharmaceutical solubilizers [28, 29]. Desiraju et al. studied the interplay between the opposing effects on apparent solubility and permeability modified for the drug Hydrochlorothiazide cocrystals [30]. Strong molecular complexation or high binding behaviour with polar components results in substantially enhanced solubility. At the same time, the high binding constant offers very little free drug/coformer even at relatively low concentration, thereby altering membrane permeation behaviour. Thus, the solubility and membrane permeability coalesce to predict the drug absorption or in vitro bioavailability of a drug. To emphasize the effects of chemical and structural changes on solubility, diffusion and permeability behaviour by variable stoichiometry API cocrystals, they are subjected for membrane permeability determination using diffusion methods and further compared with THP·*m*-ABA and/or THP·*p*-ABA cocrystals.

Permeability experiments on THP·*o*-ABA variable stoichiometry cocrystals indicate all exhibited improved permeability compared to the parent THP. The permeation behavior for THP·*m*-ABA and THP·*o*-ABA cocrystals are also evaluated. Though THP·*m*-ABA cocrystal showed better diffusion in comparison with THP·*p*-ABA cocrystal, both express low permeation and solubility that are comparable to the API. Exercising crystal structures we detected THP·*m*-ABA, THP·*p*-ABA cocrystals are not comprised of THP···THP, N−H···O hydrogen-bonded homodimer. In fact crystal structure of THP form II does not contain this dimer motif. It is apparent that the presence of stable THP···THP, N−H···O dimer offers weaker interactions with nearby molecules suggesting a higher solubility and dissolution. Moreover, THP···THP N−H···O homodimer formation in later two cocrystals are not observed, which can be suggested for their low permeation behaviour. A careful examination of THP·*o*-ABA cocrystal structure revealed that the COOH group (the best donor, pK_a = 4.95) is hydrogen bonded to the imidazole N (the best acceptor, pK_a = 8.60) supported by an auxiliary weak C−H···O interaction resulting $R_2^2(7)$ hydrogen-bonded motif (Synthon 1, Figure 3.13a). However, THP cocrystals with *m*-ABA and *p*-ABA depicted the acid-

amide like heterodimers of $R_2^2(9)$ motif (Synthon 2, Figure 3.13b). Hydrogen bond synthon energies for the synthon 1 & 2 are calculated using Gaussian09, B3LYP/6-311G*(d,p) basis level. Synthon 1 (E = −14.177 Kcalmol^{-1}) is found to be marginally weaker than synthon 2 (E = −17.444 Kcalmol^{-1}). The existence of stronger synthon **2** in THP•*m*/*p*-ABA cocrystals possibly the reason for bringing down solubility and permeability of the cocrystals.

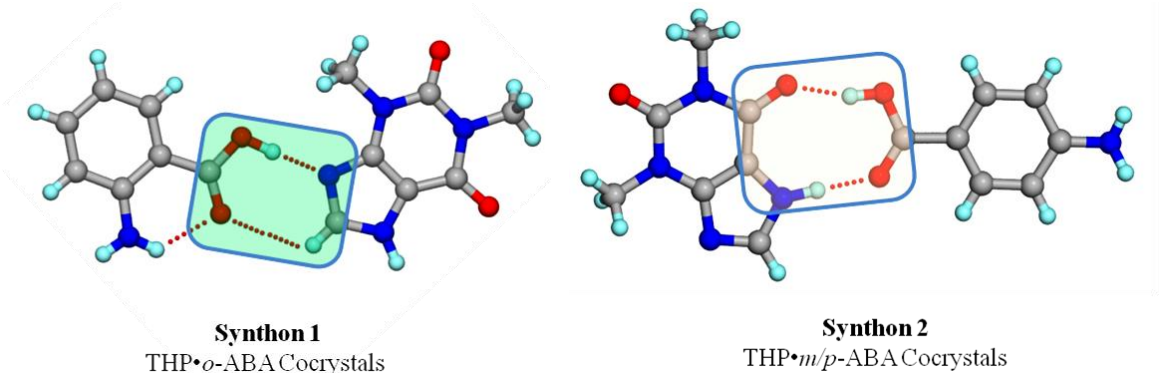

(a) (b)

Figure 3.13 (a) The coformer o-ABA interactions with the API, THP showing $R_2^2(7)$ hydrogen-bonded motif in THP·o-ABA stoichiometry cocrystals, (b) whereas m/p-ABA forms $R_2^2(9)$ hydrogen-bonded motif

It is observed from the crystal structures that CC-I and CC-IV exhibited two distinct molecular ribbons leaving the cavities for solvent inclusion depicted in Figure 3.5 & 3.8a. The structure CC-III is found as a hybrid of CC-I and CC-IV which may explain its intermediate permeability (Figure 3.14). Moreover, the permeability of a drug broadly depends upon the non-polar interactions on the crystal's surface by the non-polar cell membranes during diffusion. The THP·*o*-ABA stoichiometry cocrystals offered layered structures comprised of either cavity or channels that promoted solvent inclusion. Therefore we believe the hydrophobic (π···π/H···π) and hydrophilic (N/O···H) combined interactions may be guiding in improving the aqueous permeability of the drug in the form of cocrystal. The polarity of water is crucial and reflected in lower permeability behaviour for CC-III & CC-IV. One NH seems to be not strongly bonded with any acceptor in structure CC-VI increases the polar nature of the cocrystals while comparing CC-V. This resulted in a sudden drop of permeation behaviour of CC-VI. Thus the role of supramolecular hydrogen bond synthons, solute···solvent interactions and

hydrophobic···polar component interactions explains the interplay of solubility order i.e. CC-I>CC-II>CC-III>CC-IV and permeability order, i.e. CC-II> CC-IV> CC-III> CC-I.

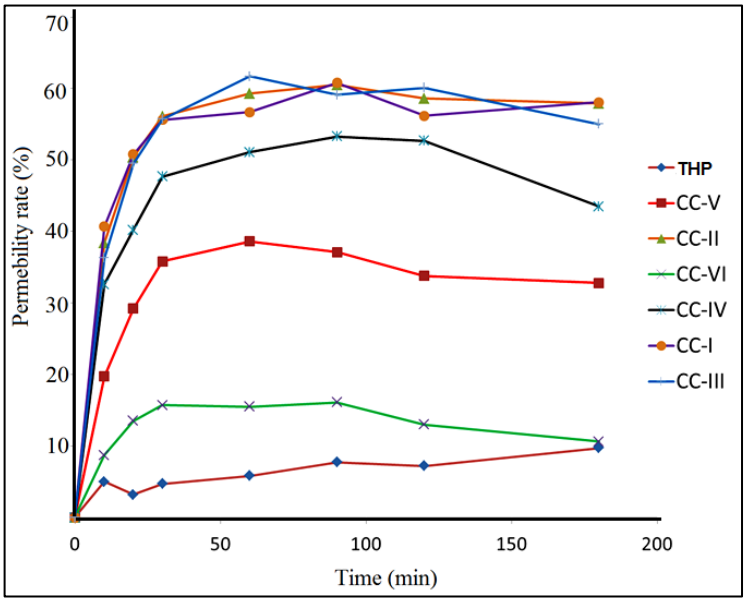

Figure 3.14 Membrane permeability profiles of the drug THP, coformer *o*-ABA and their variable stoichiometry cocrystals (CC-I, CC-II, CC-III and CC-IV). Permeability profiles for CC-V and CC-VI are also evaluated for comparison.

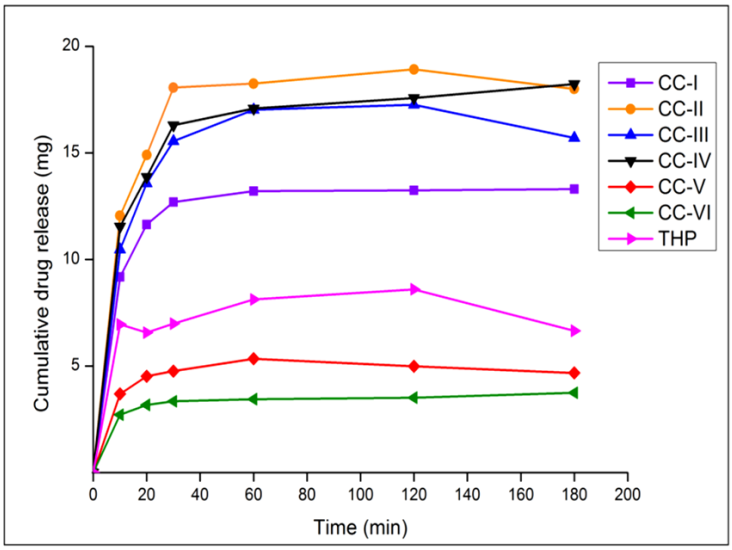

Figure 3.15 Cumulative amount of THP drug and their cocrystals diffused vs. time plot

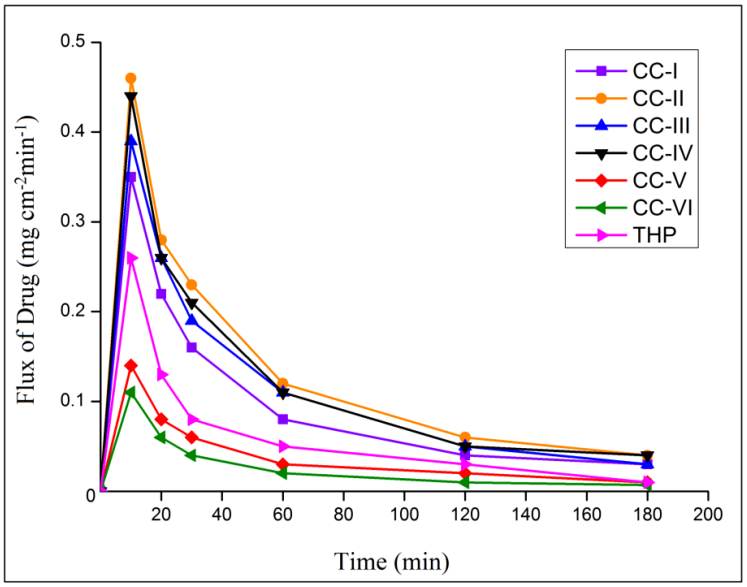

Figure 3.16 Plots of flux/permeability of the cocrystals with respect to time

The cumulative amount of THP drug release (Figure 3.15) and plots of flux/permeability of the cocrystals (Figure 3.16) with respect to the time indicated slow release and lower flux density for CC-V and CC-VI. This observation is again dictated the interplay of polar coformers and/or solvent molecules interact with the media and formation of hydrogen-bonded synthons.

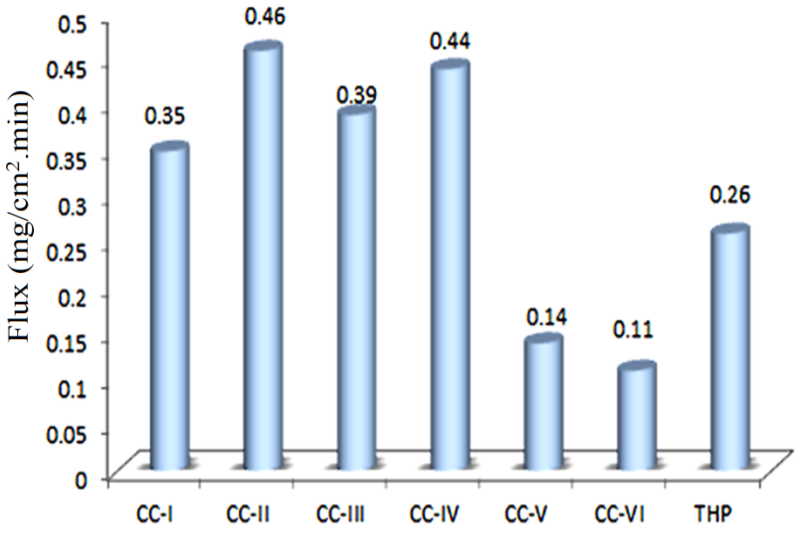

Figure 3.17 Flux of drug THP and cocrystals measured at 3 h indicate the superiority of *o*-ABA cocrystals but inferiority with *m/p*-ABA cocrystals over the drug.

The flux of the drug cocrystals were calculated and found superior for THP·*o*-ABA cocrystals and linked such observations to solute···solvent interactions and supramolecular synthon formation between drug···coformer (Figure 3.17). Higher soluble cocrystal CC-I is found to be the lower bio-available drug while comparing with other ratio cocrystals suggesting the amount of coformer present in variable ratio cocrystals is not only the reason for variable bioavailability. Molecular packing in the crystals, supramolecular synthon formation, types of included guest, drug···coformer and solute···solvent interactions and their interplay are realized as important contributors toward the desired bioavailability of the drug. For a better understanding how interactions between drug···coformer, solute···solvent and included guest molecules effect on the overall bioavailability of the API, a quantitative analysis of various interactions between components has been carried out using Hirshfeld surface analysis tools.

3.3.6 Hirshfeld Surface Analysis

Analysis of molecular crystal structures using Hirshfeld surfaces has increasingly gained in popularity because it calculates internuclear distances, angles, and identifies intermolecular interactions which deemed to be very important in structure-activity research [31, 32]. The 2-D fingerprint plots, which are derived from the Hirshfeld surfaces, are unique for each cocrystal. The histogram plotted in Figure 3.18 signifies the quantitative amount of various intermolecular interactions for CC-I to CC-VI cocrystals. Hirshfeld analysis on CC-II is performed using PLATON Squeezed structure. Thus the interaction parameter showed in the diagram may vary from the actual. The contribution of strong O···H interaction in the THP·*o*-ABA cocrystals is found higher for CC-IV (the solubility order for the cocrystals I >IV> III). This suggests lower solubility but better permeation property and bioavailability while comparing CC-I. When we compared the crystal structure of polymorph-II of THP and THP·*m*/*p*-ABA cocrystals, we observe that the N−H···O hydrogen-bonded dimer is absent. The form II of THP show catemer and has $R_2^2(8)$ motif. Whereas form IV showed N−H···O dimer and has $R_2^2(10)$ motif. Dimers are generally discrete and linked to other dimers only by weak C−H···O and C−H···N. supported by π···π stacking parallel to (001) axis. The dimer is similar to the motif observed in the monohydrate and in a number of theophylline cocrystals (nearly

32.5%). The presence of this dimer motif in the thermodynamically stable form IV and theophylline monohydrate, considered to be the most stable structure in an aqueous environment, may account for the thermodynamic stability of this structural motif compared to the chain motif of form II. In THP·*o*-ABA cocrystals, the THP dimer is present but remains discrete and shows weaker drug···coformer or cocrystal···solvent interactions. This emphasizes in improved solubility and drug release property for THP·*o*-ABA cocrystals. Thus the present work demonstrated a link of intermolecular interactions in cocrystals and different stoichiometry cocrystals with respect to their solubility and drug release behaviour.

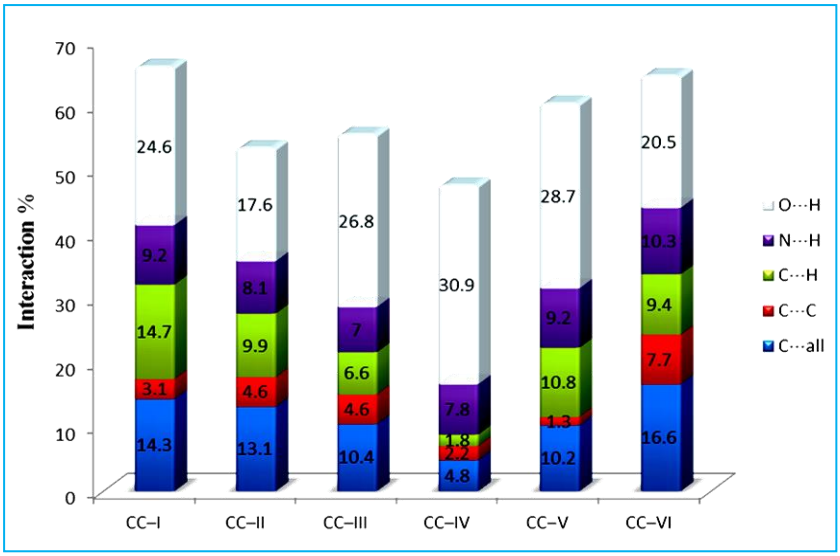

Figure 3.18 Percentage of intermolecular interactions calculated using Hirshfeld surface area analysis in cocrystals CC-I to CC-VI. The actual interactions contribution evaluated for CC-II may slightly differ as PLATON Squeezed structure is the input for calculation. Contribution from two molecules of *iso*-BuOH needed to consider.

3.4 Summary

In this chapter drug theophylline (THP), is considered as a model system to prepare variable stoichiometry cocrystals by utilising crystal engineering principles. Isomeric aminobenzoic acids are chosen as coformers, which also have biological importance. Six new cocrystals of theophylline is synthesized using solvent assisted mechanochemical grinding. Aqueous solubility and membrane permeability are studied. This is to establish different stoichiometry cocrystals show different physicochemical properties. All cocrystals exhibited enhanced solubility, which is attributed to a possible polarity change caused by cocrystallization. Flux/permeability studies of four different stoichiometry

cocrystals of THP·*o*-ABA, through 'dialysis membrane', showed enhanced flux/permeability. Non-solvated 2:3 cocrystal of THP·*o*-ABA [CC-I] showed the highest solubility and is attributed to the formation of weaker N−H···O interaction with the coformers. Drug cocrystals with *o*-Aminobenzoic acid coformer showed the COOH group (the best donor) which is hydrogen bonded to the imidazole N (best acceptor) supported by auxiliary weak C−H···O interaction $R_2^2(7)$. However, THP cocrystals with *m*-ABA and *p*-ABA depicted the acid-amide like heterodimers of $R_2^2(9)$ motif. Adjustment of COOH to THP hydrogen-bonded motifs plays an important role to modulate solubility and permeability of the cocrystals. A Hirshfeld surface analysis is carried out and showed a correlation between drug···coformer interactions (heterosynthon) of the cocrystals with the product of permeability and solubility, i.e. effective bioavailability of the drug. The trade-off between solubility increase and permeability decrease between stoichiometric cocrystals is emphasized and correlated with the participation of various supramolecular interactions. Therefore, the present study provides an understanding of how weak interactions and/or supramolecular synthons play a decisive role to alter the stoichiometry of cocrystals of an API and consequently the physiochemical properties.

3.5 Experimental Section

3.5.1 Materials

Drug theophylline (purity ≥99%, Sigma Aldrich) and the coformer isomeric Aminobenzoic acids are purchased from Sigma Aldrich and used as received. The analytical-grade solvents used for the studies are obtained from Merck and used without further purification. Millipore water is used to carry out crystallization, solubility, diffusion/permeability experiments.

3.5.2 Preparation of Cocrystals

Suitable crystals of THP and ABA at different ratios are grown by liquid assisted mechanochemical grinding for 45 minutes for *o*-ABA coformer followed by slow evaporation of solutions from the reactant mixtures. Various common laboratory solvents are used and crystallization is carried out at ambient conditions. Combinations of different ratio starting materials are attempted to corroborate if any new cocrystal

material is formed. Four distinct different ratio THP and *o*-ABA cocrystals are isolated from nearly 51 crystallizations using 17 different individual solvents and/or solvent mixtures (Table 3.5). Same has been repeated for *m*-ABA and *p*-ABA but only the formation of 1:1 cocrystal is observed.

Table 3.5 Mechanochemical grinding THP and isomeric ABAs mixtures result in cocrystals. Three different starting drug-coformer ratios and 17 solvent systems are examined to afford various stoichiometry cocrystals. Only *o*-ABA results in four different stoichiometry cocrystals. The *m*-ABA and *p*-ABA show only 1:1 cocrystal irrespective of starting material ratio and solvent of crystallization.

Crystallization Solvent	**THP:ABA**	**THP+*o*-ABA**	**THP+*m*-ABA**	**THP+*p*-ABA**
		Cocrystal formation	**Cocrystal formation**	**Cocrystal formation**
Acetonitrile	1:1	CC-I*	CC-V	CC-VI
	1:2	IC	CC-V*	IC
	2:1	IC	CC-V*	CC-VI
Methanol	1:1	CC-I*	CC-V	CC-VI
	1:2	CC-IV*	CC-V*	IC
	2:1	CC-IV	CC-V	CC-VI
Ethanol	1:1	CC-I	CC-V	CC-VI
	1:2	CC-I*	IC	IC
	2:1	CC-IV	CC-V*	CC-VI
Iso-BuOH	1:1	CC-II	CC-V	CC-VI
	1:2	CC-II*	IC	IC
	2:1	CC-II*	CC-V*	CC-VI*
Water	1:1	CC-III*	IC	CC-VI*
	1:2	CC-III*	IC	CC-VI*
	2:1	CC-III	IC	CC-VI
1,4-Dioxane	1:1	IC	IC	IC
	1:2	IC	IC	IC
	2:1	IC	IC	IC
Diethyl ether	1:1	IC	IC	IC
	1:2	IC	IC	IC
	2:1	IC	IC	IC
Dichloromethane	1:1	IC	CC-V	VI
	1:2	IC	CC-V*	CC-VI*
	2:1	IC	CC-V*	CC-VI*
Chloroform	1:1	IC	CC-V*	IC
	1:2	IC	CC-V*	IC
	2:1	IC	CC-V*	IC
Acetone	1:1	IC	IC	IC

	1:2	IC	IC	IC
	2:1	IC	IC	IC
Acetic acid	1:1	IC	IC	IC
	1:2	IC	IC	IC
	2:1	IC	IC	IC
Tetrahydrofuran	1:1	IC	IC	IC
	1:2	IC	IC	IC
	2:1	IC	IC	IC
1-Propanol	1:1	CC-I	CC-V	CC-VI
	1:2	CC-I*	CC-V*	CC-VI*
	2:1	CC-I*	CC-V*	CC-VI*
2-Propanol	1:1	CC-I	CC-V	CC-VI
	1:2	CC-I*	CC-V*	CC-VI*
	2:1	CC-I*	CC-V*	CC-VI*
Acetonitrile + 2-Propanol	1:1	CC-I	CC-V	CC-VI
	1:2	CC-I*	CC-V*	CC-VI*
	2:1	CC-I*	CC-V*	CC-VI*
Chloroform + Methanol	1:1	CC-I	CC-V	CC-VI
	1:2	CC-I*	CC-V*	CC-VI*
	2:1	CC-I*	CC-V*	CC-VI*
Chloroform + Ethanol	1:1	CC-I	CC-V	CC-VI
	1:2	CC-I*	CC-V*	CC-VI*
	2:1	CC-I*	CC-V*	CC-VI*

* Incomplete conversion of the cocrystal, IC = individual components

3.5.3 Vibrational Spectroscopy

A Nicolet 6700 FT-IR spectrometer with a NXR FT-Raman Module is used to record the IR spectra. The IR spectra are recorded on samples dispersed in a KBr pellets. All major stretching vibrations for cocrystals, **CC-I**: 3467 (O–H), 3363 (N–H), 1690 (C=O, C=N), 1300 (C–N), 851 (N–C–H); **CC-II**: 3470 (O–H), 3369 (N–H), 1668 (C=O, C=N), 1302 (C–N), 1241 (C–O), 854 (N–C–H); **CC-III**: 3538 (O–H), 3489 (N–H), 1698, (C=O, C=N), 1299 (C–N), 1237(C–O), 856 (N–C–H); **CC-IV**: 3536 (O–H), 3476 (N–H), 1678 (C=O, C=N), 1301 (C–N), 1239 (C–O), 854 (N–C–H); **CC-V**: 3442(O–H), 3356(N–H), 2469 and 1927 (O–H···N), 1697(C=O), 1336(C–O), 864(N–C–H); **CC-VI**: 3475 (O–H), 3386 (N–H), 1706 (C=O), 1255 (C–O), 844 (N–C–H) cm^{-1}.

3.5.4 Differential Scanning Calorimetry (DSC)

DSC thermograms of cocrystals are performed on a Mettler Toledo DSC 822e module. The instrument is calibrated for temperature and heat flow accuracy using the melting of pure indium (mp 156.6°C and ΔH of 25.45 Jg^{-1}). Samples are placed in crimped but vented aluminium sample pans for DSC. A typical sample size of 4–6 mg is taken with temperature range of 30–300 °C at 5°C min^{-1}. The representative melting temperature onsets of the cocrystals and corresponding solvate/water release onsets are examined (Table 3.2).

3.5.5 Thermal Gravimetric Analysis (TGA)

The TGA scans are obtained on a Mettler Toledo TGA/SDTA 851e module. TGA traces are recorded at a heating rate of 10 °C min^{-1} under a nitrogen purge of 30 mL min^{-1}. Samples with masses between 9-10 mg are analysed by using aluminium pans. Mass loss (%) is calculated based on the mass of the original sample.

3.5.6 Single Crystal X-ray Diffraction

X-ray reflections are collected on a Bruker APEX-II, CCD diffractometer using Mo Kα (λ = 0.71073 Å) radiation. Data reduction is performed using Bruker SAINT Software [30]. Intensities for absorption are corrected using SADABS. Structures are solved and refined using SHELXL-2014 with anisotropic displacement parameters for non-H atoms [31]. Hydrogen atoms on O and N are experimentally located in all crystal structures. All C–H atoms are fixed geometrically using the HFIX command in SHELX-TL. X-Seed is used to prepare figures and packing diagrams [32]. A check of the final CIF file using PLATON did not show any missed symmetry [33,34]. The crystallographic parameters for all structures are summarized in Appendix Table A.4. The hydrogen bond distances in the X-ray crystal structures (Table 3.3) are neutron-normalized by fixing the D–H distance to its accurate neutron value (O–H 0.983 Å, N–H 1.009 Å, C–H 1.083 Å).

3.5.7 Phase Stability Determination

Isolated pure cocrystals of CC-I and CC-III are taken after grinding crystals to a fine powder into a 10 mL beaker. Approximately 2–4 mL of Millipore water is added to prepare slurry for CC-I and CC-III. The slurries are kept stirring (~80 rpm) at ambient condition for 3 days (25 °C). A definite amount of the slurry sample is taken out of the

beaker at time intervals of 1, 24, 48, and 72 h; the sample is air-dried and then submitted for powder X-ray diffraction (PXRD) data analysis. The stacked plot of PXRD patterns is presented to study whether the solvent (water) mediated phase transformation occurred and is discussed in the Results and Discussion section.

3.5.8 Solubility Determination

UV-Vis spectroscopy is used to determine the solubility of all cocrystal materials prepared. All experiments are performed in a HALO DB-30 UV-visible double beam spectrophotometer. The experiment for unknown concentration solutions is repeated for three times. The concentration of the unknown solution (C_u) of the cocrystal is evaluated from the slope and intercept of the calibration curve by using the formula $C_u = (A_u – \text{Intercept})/\text{Slope}$, where A_u is the absorbance of the unknown solution. Gravimetric measurements were performed (2 mL at regular interval) to compare solubility parameter extracted from UV-Vis calibration curves and found in order.

3.5.9 Membrane Permeability Determination

The diffusion studies of THP and its cocrystals are carried out through a dialysis membrane-135' [Dialysis Membrane-135 Average flat width - 33.12 mm, Average diameter - 23.8 mm, capacity approx. - 4.45 ml/cm] obtained from HiMedia, India; using a diffusion apparatus. The dialysis membrane is pre-treated with 2% of $NaHCO_3$ at 80 °C for 30 min to remove traces of sulfides, followed by 10 mM of EDTA at 80 °C for 30 min to remove the traces of heavy metal and another 30 min of treatment with deionised water at 80 °C to remove glycerine. The treated dialysis membrane is mounted in clips and placed suspensions of the drug THP and its cocrystal materials at concentration 20 mg/mL. The drug and/or cocrystal solution is then allowed to rotate at 45 rpm and diffuse through the membrane towards the receptor compartment containing 150 mL Phosphate-buffered saline (PBS, pH=7.4). The release of the compounds at the receptor compartment through dialysis tube is analysed by UV−Vis spectrophotometer at a λ_{max} of 270 nm after suitable dilution and at different time intervals up to 3 hrs. An aliquot of 2 mL of the sample is withdrawn from the receptor compartment at time 0, 10, 20, 30, 60, 90, 120 and 180 minutes. The receptor compartment solution volume is kept constant by replacing fresh medium.

3.6 References

[1] Trask, A. V., Van De Streek, J., Motherwell, W. D. S., and Jones, W. Achieving polymorphic and stoichiometric diversity in cocrystal formation: Importance of solid-state grinding, powder X-ray structure determination, and seeding. *Crystal Growth and Design*, 5(6):2233-2241, 2005.

[2] Karki, S., Friščič, T., and Jones, W. Control and interconversion of cocrystal stoichiometry in grinding: Stepwise mechanism for the formation of a hydrogen-bonded cocrystal. *CrystEngComm*, 11(3):470-481, 2009.

[3] Seaton, C. C., Parkin, A., Wilson, C. C., and Blagden, N. Controlling the formation of benzoic acid: Isonicotinamide molecular complexes. *Crystal Growth and Design*, 9(1):47-56, 2009.

[4] Jayasankar, A., Reddy, L. S., Bethune, S. J., and Rodríguez-Hornedo, N. Role of Cocrystal and Solution Chemistry on the Formation and Stability of Cocrystals with Different Stoichiometry. *Crystal Growth & Design*, 9(2):889-897, 2009.

[5] Leyssens, T., Springuel, G., Montis, R., Candoni, N., and Veesler, S. Importance of solvent selection for stoichiometrically diverse cocrystal systems: Caffeine/maleic acid 1:1 and 2:1 cocrystals. *Crystal Growth and Design*, 12(3):1520-1530, 2012.

[6] Li, Z. and Matzger, A. J. Influence of Coformer Stoichiometric Ratio on Pharmaceutical Cocrystal Dissolution: Three Cocrystals of Carbamazepine/4-Aminobenzoic Acid. *Molecular Pharmaceutics*, 13(3):990-995, 2016.

[7] Abourahma, H., Shah, D. D., Melendez, J., Johnson, E. J., and Holman, K. T. A Tale of Two Stoichiometrically Diverse Cocrystals. *Crystal Growth and Design*, 15(7):3101-3104, 2015.

[8] Bora, P., Saikia, B., and Sarma, B. Regulation of π···π Stacking Interactions in Small Molecule Cocrystals and/or Salts for Physiochemical Property Modulation. *Crystal Growth and Design*, 18(3):1448-1458, 2018.

[9] Sarma, B., Sreenivas Reddy, L., and Nangia, A. The role of π-stacking in the composition of phloroglucinol and phenazine cocrystals. *Crystal Growth and Design*, 8(12):4546-4552, 2008.

[10] Oh, S. Y., Nickels, C. W., Garcia, F., Jones, W., and Friščić, T. Switching between halogen- and hydrogen-bonding in stoichiometric variations of a cocrystal of a phosphine oxide. *CrystEngComm*, 14(19):6110-6114, 2012.

[11] Kulkarni, C., Wood, C., Kelly, A. L., Gough, T., Blagden, N., and Paradkar, A. Stoichiometric Control of Co-Crystal Formation by Solvent Free Continuous Co-Crystallization (SFCC). *Crystal Growth and Design*, 15(12):5648-5651, 2015.

[12] Wang, J. R., Bao, J., Fan, X., Dai, W., and Mei, X. pH-Switchable vitamin B9 gels for stoichiometry-controlled spherical co-crystallization. *Chemical*

Communications, 52(92):13452-13455, 2016.

[13] Bolla, G. and Nangia, A. Pharmaceutical cocrystals: Walking the talk. *Chemical Communications*, 52(54):8342-8360, 2016.

[14] Qiao, N., Li, M., Schlindwein, W., Malek, N., Davies, A., and Trappitt, G. Pharmaceutical cocrystals: An overview. *International Journal of Pharmaceutics*, 419(1-2):1-11, 2011.

[15] Steed, J. W. The role of co-crystals in pharmaceutical design. *Trends in Pharmacological Sciences*, 34(3):185-193, 2013.

[16] Thakuria, R., Delori, A., Jones, W., Lipert, M. P., Roy, L., and Rodríguez-Hornedo, N. Pharmaceutical cocrystals and poorly soluble drugs. *International Journal of Pharmaceutics*, 453(1):101-125, 2013.

[17] Duggirala, N. K., Perry, M. L., Almarsson, Ö., and Zaworotko, M. J. Pharmaceutical cocrystals: along the path to improved medicines. *Chemical Communications*, 52(4):640-655, 2016.

[18] Corner, P. A., Berry, D. J., McCabe, J. F., Barbas, R., Prohens, R., Du, H., Zhou, H., and Llinas, A. Property prediction and pharmacokinetic evaluation of mixed stoichiometry cocrystals of zafirlukast, a drug delivery case study. *CrystEngComm*, 20(10):1346-1351, 2018.

[19] Saikia, B., Bora, P., Khatioda, R., and Sarma, B. Hydrogen Bond Synthons in the Interplay of Solubility and Membrane Permeability/Diffusion in Variable Stoichiometry Drug Cocrystals. *Crystal Growth and Design*, 15(11):5593-5603, 2015.

[20] Bhogala, B. R., Basavoju, S., and Nangia, A. Three-component carboxylic acid-bipyridine lattice inclusion host. Supramolecular synthesis of ternary cocrystals. *Crystal Growth and Design*, 5(5):1683-1686, 2005.

[21] Sarma, B., Nath, N. K., Bhogala, B. R., and Nangia, A. Synthon competition and cooperation in molecular salts of hydroxybenzoic acids and aminopyridines. *Crystal Growth and Design*, 9(3):1546-1557, 2009.

[22] Sarma, B. and Saikia, B. Hydrogen bond synthon competition in the stabilization of theophylline cocrystals. *CrystEngComm*, 16(22):4753-4765, 2014.

[23] Madusanka, N., Eddleston, M. D., Arhangelskis, M., and Jones, W. Polymorphs, hydrates and solvates of a co-crystal of caffeine with anthranilic acid. *Acta Crystallographica Section B: Structural Science, Crystal Engineering and Materials*, 70(1):72-80, 2014.

[24] Bevill, M. J., Vlahova, P. I., and Smit, J. P. Polymorphic cocrystals of nutraceutical compound p -coumaric acid with nicotinamide: Characterization, relative solid-state stability, and conversion to alternate stoichiometries. *Crystal Growth and Design*, 14(3):1438-1448, 2014.

[25] Schultheiss, N. and Newman, A. Pharmaceutical Cocrystals and Their Physicochemical Properties. *Crystal Growth & Design*, 9(6):2950-2967, 2009.

[26] Fernandes, J. A., Sardo, M., Mafra, L., Choquesillo-Lazarte, D., and Masciocchi, N. X-ray and NMR Crystallography Studies of Novel Theophylline Cocrystals Prepared by Liquid Assisted Grinding. *Crystal Growth and Design*, 15(8):3674-3683, 2015.

[27] Trask, A. V., Motherwell, W. D. S., and Jones, W. Physical stability enhancement of theophylline via cocrystallization. *International Journal of Pharmaceutics*, 320(1-2):114-123, 2006.

[28] Aitipamula, S., Wong, A. B. H., Chow, P. S., and Tan, R. B. H. Cocrystallization with flufenamic acid: Comparison of physicochemical properties of two pharmaceutical cocrystals. *CrystEngComm*, 16(26):5793-5801, 2014.

[29] Eddleston, M. D., Madusanka, N., and Jones, W. Cocrystal Dissociation in the Presence of Water: A General Approach for Identifying Stable Cocrystal Forms. *Journal of Pharmaceutical Sciences*, 103(9):2865-2870, 2014.

[30] *SAINT Plus, Bruker AXS Inc.: Madison, WI*. 2008.

[31] *BRUKER AXS (v 6.14); Bruker AXS Inc.: Madison, WI*. 2008.

[32] L. J. Barbour *X–Seed, Graphical Interface to SHELX–97 and POVRay University of Missouri–Columbia*. 1999.

[33] Spek, A. L. *PLATON, A Multipurpose Crystallographic Tool Utrecht University, Utrecht, Netherland*. 2002.

[34] Spek, A. L. and IUCr Single-crystal structure validation with the program *PLATON*. *Journal of Applied Crystallography*, 36(1):7-13, 2003.